Prepared for submission to JINST

Performance of a capillary-tube fibre-based dual-readout calorimeter

E-mail: i.vivarelli@sussex.ac.uk

Keywords: Dual-readout calorimetry, Cherenkov light, optical fibres, SiPM

Contents

1 Introduction

Dual-readout calorimetry [1] is a compelling technique, actively investigated by several groups as an option to reach excellent hadronic calorimetric resolution at future lepton colliders, (such as, for instance, FCC-ee and CEPC [2, 3]).

Dual-readout calorimetry operates on the principle of dual signal sampling within a calorimeter, utilizing two distinct sensitive materials characterized by differing h/e ratios. By combining the information from these two signals, this approach effectively compensates for fluctuations in the electromagnetic fraction of hadronic showers, thereby significantly enhancing the accuracy of energy measurements and restoring linearity in the calorimeter's response to hadrons. This technique [1] is well-established, with its feasibility confirmed through an extensive experimental program spanning two decades [4–9]. The outcome of this programme is a design that incorporates two types of optical fibers embedded within an absorber, oriented nearly parallel to the trajectory of incoming particles. Scintillating fibers sample the charged particles in the shower, while undoped plastic fibers collect Cherenkov light predominantly produced by electrons and positrons, providing sensitivity to the electromagnetic shower component.

Recent advancements in dual-readout technology include the integration of silicon photomultipliers (SiPMs) as light detectors capable of reading individual fibers [10]. Simulations of a comprehensive 4π dual-readout calorimeter[1] have been documented both using the calorimeter as a standalone device to measure the energy of both electrons/photons and hadrons [11, 12], and in conjunction with a crystal-based dual-readout electromagnetic section positioned ahead of the fibre-based calorimeter hadronic calorimeter [13, 14]. The combined crystal + fibre based calorimeter shows great potential in terms of energy resolution to hadrons: Ref. [14] estimated the performance of a simple particle flow algorithm on top of the dual-readout calorimeter response, obtaining jet energy resolutions of $\sigma/E \sim 30\%/\sqrt{E\ [\mathrm{GeV}]}$. The combined crystal + fibre configuration is now the baseline for the IDEA detector concept [15].

This study focuses on a second test-beam of a prototype designed with a recently explored mechanical construction concept: optical fibres are housed in individual cylindrical brass capillary tubes, which are then glued together to form calorimeter modules. This design offers a cost-effective and flexible solution for large-scale construction. The prototype construction is documented in Ref. [16]. Its size guarantees a good containment for electromagnetic showers, but only a poor one for hadronic showers. A first assessment of the quality of the prototype response to positrons was done in Ref. [17] in terms of linearity and resolution of the energy measurement, and of the quality of the shower profile measurement. However, a poor positron beam purity and a non optimal placement of one of the auxiliary detectors limited the ability to assess the energy resolution at positron beam energies higher than $E_{\mathrm{beam}} = 30$ GeV. Moreover, the lack of a vertical tilt angle between the beam and the calorimeter axis introduced a dependency of the response on the particle impact point on the calorimeter, which had to be corrected at the analysis level. These issues forced the use of the software simulation to make a statement on the optimal calorimeter energy resolution.

All these issues were solved in a second test-beam, performed in 2023 at the H8 beam line at the CERN SPS. This paper describes the results of this second test-beam, in terms of linearity and resolution of the prototype energy response to positrons from 10 to 120 GeV.

Section 2 provides an overview of the experimental setup, including the calorimeter structure, readout system, and auxiliary detectors used to isolate electrons within the beam. The optimisation of the positron selection and estimated positron beam purities are described in Section 3. The calibration procedure, detailing the equalization of module responses and electromagnetic scale calibration, is outlined in Section 4. The calorimeter's response to positrons is presented in Section 5, with concluding remarks in Section 6.

2 Experimental setup

The prototype tested on beam is the same as the one tested in 2021. It is described in detail in Ref. [17]. The prototype is shown in Figure 1.

Nine identical modules, labelled as $\mathrm{M}_[0] - \mathrm{M}_8$ are arranged as shown in Figure 1. Each module is 100-cm long and its dimensions transverse to the beam are 3.3×3.3 cm^2, yielding a total prototype size of about $100 \times 10 \times 10$ cm^3. Each module is assembled by gluing together 320 100-cm long brass (63% Cu, 37% Zn) capillary tubes. Each tube encloses a 100-cm long optical fibre. The dual readout is obtained by utilising two different sets of fibres: one set of scintillating

[1] in this case, the mechanical and geometrical configurations was different from the one with capillary tubes discussed in this paper. Still, the results are worth to be mentioned here as a benchmark of what can be achieved with a dual-readout calorimeter

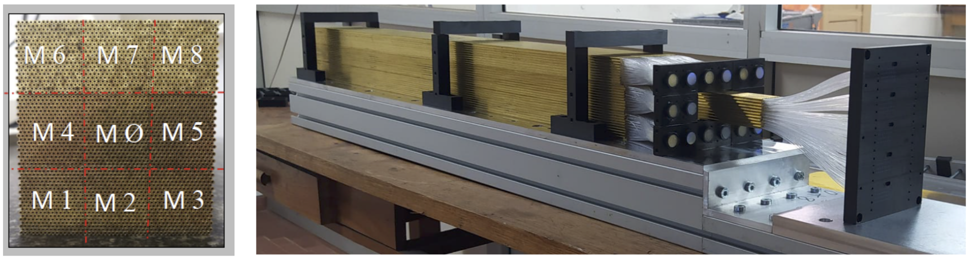

Figure 1. View of the prototype and its segmentation in the $M_0 - M_8$ modules.

and one of clear undoped fibres. The scintillating fibres (BCF-10 from Saint Gobain [18]) have a polystyrene-based core and a single PMMA clad. The emission peak is at 432 nm, and the light yield is about 8000 photons per MeV. The clear undoped fibres (referred to as "Cherenkov" in the following) are SK-40 from Mitsubishi [19]. They have a PMMA resin core and a fluorinated polymer clad, and a numerical aperture of 0.5.

Overall, the volumes of the prototype are 66% brass, 11% fibres, with air and glue covering the rest. The effective radiation length is estimated to be 22.7 mm, while the Molière radius is 23.8 mm. The alternating layout of the scintillating and Cherenkov fibres is shown in Figure 2(b).

The external modules $M_1 - M_8$ are instrumented with Hamamatsu R8900 PMTs [20]. The scintillating and clear fibres are separated and bundled in two groups on the back side of each module to match the PMTs' window. A yellow filter (Kodak Wratten 3, with nominal transmission of about 7% at 425 nm and 90% at 550 nm) is placed between the scintillating fibres and the detector to attenuate the scintillation signal and to cut off short wavelength components of the light: this helps reducing the calorimeter response dependence on the shower depth and starting point by selecting wavelengths with a longer fibre attenuation length. The PMTs are read out with V792AC QDC modules produced by CAEN S.p.A..

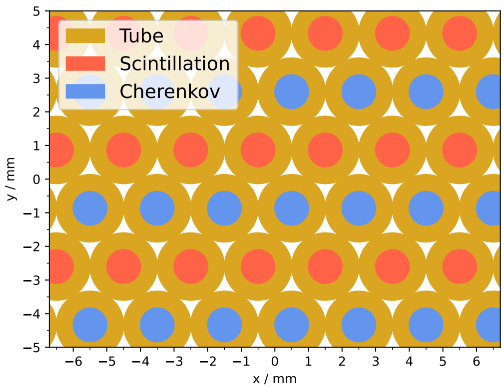

Figure 2. Sketch of the front face of the calorimeter detailing the relative positions of the Cherenkov and scintillating fibres.

Each individual fibre of the central module M_0 is instead read out by an individual SiPM with a 1.3×1.3 mm^2 sensitive area. The SiPMs (S14160-1315 PS [21]) have a pitch of 15 μm, for a total number of cells of 7284. The fibres at the back of the calorimeter drive the light to front-end boards, each hosting 64 SiPMs. The front-end board is split in two optically-insulated groups to avoid optical cross-talk between the Cherenkov and scintillating light. As for the modules $M_1 - M_8$, yellow filters are placed between the scintillating fibres and the SiPMs. In addition, for M_0 a transparent paper is used between the clear fibres and the SiPMs for mechanical reason and to avoid any air gap between the fibres and the light sensors.

The SiPM readout is based on the FERS system produced by CAEN S.p.A. [22], based on the Citiroc 1A [23] chip. Each readout board (A5202) is equipped with two Citiroc 1A to operate 64 SiPMs. The signal produced by each SiPM feeds two charge amplifiers (named High-gain, or HG, and Low-gain, LG in the following) with tunable gains. The gain of the HG is set to be roughly ten times that of the LG. Both signals are read out simultaneously and stored on disk. The settings for the two charge amplifiers were chosen to guarantee good quality HG spectra and a wide dynamic range, while maintaining an overlap between the signals acquired with the two different gains to be used for their mutual calibration. The settings chosen allow signals from 1 to almost 4000 p.e. to be read out. This corresponds to about 55% of the SiPM occupancy considering the microcells available in the sensitive area. The FERS system reading the SiPM from M_0 had an internal self-trigger system: the data from one of the five boards were made available for readout only if a total signal of at least 4 p.e. was present on the board check this number. This caused no bias on the energy readout.

2.1 Beam setup

A set of auxiliary detectors present on the beam line were used as trigger system and to help particle identification. The setup was similar to that described in Ref. [17]. Figure 3 sketches the beam setup.

- Upstream the beam, two Cherenkov threshold counters [24] were available. The pressure of the He gas was set to optimise the separation between electrons and pions depending on the beam energy. The Cherenkov counters were found to be useful up to beam energies of about 40 GeV.

- A system of three scintillators was used as trigger on beam particles. The coincidence of T_1 and T_2, each 2.5 mm thick, with an area of overlap of about 4×4 cm^2 was used in anti-coincidence with a third scintillator counter (T_3), placed downstream the beam. T_3 had a 10-mm radius hole in its centre: its purpose was to veto off-axis particles. Therefore, the combination $(T_1 \wedge T_2) \wedge \bar{T}_3$ defined what will be referred to as the "physics trigger" in the following.

- A pair of Delay Wire Chambers (DWC1 and DWC2) were placed upstream and downstream the beam with respect to the trigger scintillators. They were used to determine the location of the impact point of the particles at the calorimeter surface. The typical precision that could be achieved was of a few mm.

- A preshower detector (PS in the following), consisting of 5 mm of lead and a scintillator slab read out with a photomultiplier, was located at 10 cm from the face of the calorimeter. A high-purity electron/positron selection can be achieved by requiring a signal higher than that of a MIP in the scintillator.

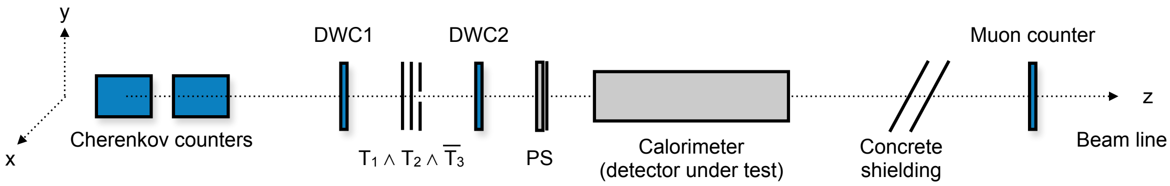

Figure 3. Sketch of the beam line setup. The diagram is not in scale.

- About 20 m downstream of the calorimeter, behind approximately eight interaction lengths of absorber, a 50×50 cm^2 scintillation counter T_μ served to identify the muons in the particle beams. This muon counter was not used in the analysis described in this paper.

Every ten physics trigger, a random "pedestal" trigger was produced. All trigger signals, physics and pedestal, were sent to two data acquisition systems, one reading the auxiliary detectors and the PMTs of modules $M_1 - M_8$, and one reading the signals from the SiPMs of the M_0 module.

The synchronisation of the two data acquisition systems was done offline, by making use of the pedestal events.

A right-handed orthogonal system of coordinates with the z-axis along the beam line, and with the y-axis pointing upwards is used in teh remainder of this paper. The origin of the coordinate system is on the front face of the calorimeter, at the geometrical centre of M_0. The calorimeter prototype was placed on beam so that its longest side formed an angle of about 1° with the z-axis in both the $x - z$ and the $y - z$ plane. This is to avoid channeling effects (particles entering and travelling long distances in an optical fibre) and to minimise any dependence of the calorimeter response on the impact point (discussed extensively in Ref. [17].

3 Particle selection

A pure beam of positrons is used for the calibration of the prototype and for the assessment of its performance of the positron energy measurement in terms of linearity and resolution as a function of the beam energy.

The positron selection starts with a selection on the DWC detectors: the aim of the selection is to avoid selecting particles that hit the calorimeter front face too far off its centre, leading to additional lateral leakage. After calibration and alignment of the DWC and the calimeters (done exploiting the excellent lateral granularity of the calorimeter thanks to the mm-level pitch of the single fibre readout), a circle with radius 6.5 mm centred in the centre of M_0 is selected in each DWC. Particles travelling at an angle with respect with the beam line are suppressed by requiring that the coordinates as read by each DWC coincide at at the level of 1.5 mm (which corresponds to a rough estimation of the DWC intrinsic resolution). This will be referred to as the "DWC selection" in the following.

The small muon component of the beam is further suppressed by requiring that the signal in the muon counter scintillator is compatible with its pedestal.

The selection of positrons is completed by the request of a large signal in both the PS and the threshold Cherenkov counters. Several selections were tested and the final one was chosen by balancing the efficiency and purity of the positron selection. The chosen selection requires a signal higher than $3\sigma_{\mathrm{ped}}$ in one Cherenkov counter and a signal compatible with that of at least three MIPs in the PS.

The equalisation and calibration of the prototype described in Section 4 were performed by using the selection described so far.

The beam purity was estimated at all energies by fitting the energy distribution in the calorimeter after energy equalisation (discussed in Section 4.2) with a third degree polynomial for the non-electron component (mainly residual hadrons) and a gaussian for the electrons. The beam purity is defined as the ratio of the integral of the gaussian peak and the total number of selected events. The resulting fit is shown in Figure 4 for E_{beam} = 40 GeV as an example.

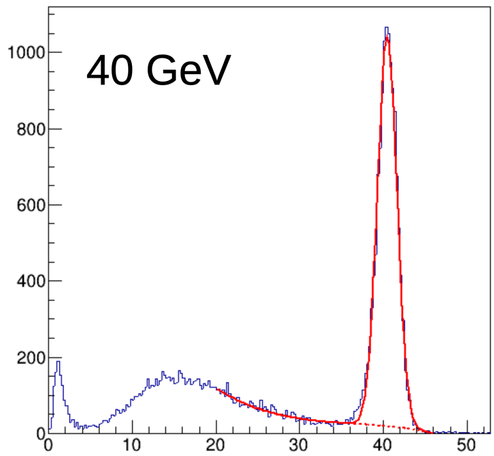

Figure 4. Energy distribution in the calorimeter (sum of Cherenkov and scintillation) after the DWC selection. The result of a fit with a third degree polynomial is shown by a dashed red line, while that of a fit with a gaussian plus a third degree polynomial is shown as a solid red line.

The beam purity estimated after applying only the DWC selection is reported in Table 1 for a subset of the energies considered. The beam purity was found to vary little between 40 and 100 GeV.

The purity was estimated again after the full positron selection described in the text. It was determined to be at least 98% at all energies considered, and above 99% for energies below 100 GeV. possible systematics associated with the residual contamination from non-positrons components on the measurements of Section 5 were evaluated to be negligible.

4 Detector calibration

The calibration of the prototype was performed in several steps steps. First, the gain of all SiPMs in M_0 was equalised, and the conversion factor between ADC counts and p.e. derived, by making

Table 1. Fraction of positrons in the beam as a function of the beam energy E_{beam}. The purity was estimated after applying the DWC selection described in the text.

E_{beam} [GeV]	Positron Purity
10	65%
20	57%
40	50%
100	46%
120	7.5%

use of the SiPM multiphoton spectrum. Then, the response of all modules M_0-M_8 was roughly equalised by making use of a positron beam with an energy of 20 GeV. After equalisation, the overall calorimeter energy scale was set by looking at the response of the whole calorimeter prototype to beams of positrons. Finally, an overall procedure is performed during the analysis. All these steps are discussed in detail below.

4.1 SiPM equalisation using the multiphoton spectrum

An ultra-fast LED emitting at 420 nm was used to perform a first SiPM equalisation in the labs before the test beam period. The same overvoltage of +7 V over the breakdown voltage was applied to all SiPMs, and the amplifier settings were tuned. The setting is not typical for a SiPM, but it guarantees a Photo Detection Efficiency (PDE) stable under small temperature variations, and a multiplication factor of $0.5 \cdot 10^6$ for each detected photon.

The multiphoton spectrum recorded with HG is the starting point of the in-situ SiPM equalisation procedure: the procedure is similar to that discussed in Ref. [17], where full details can be found.

- The peaks of the multiphoton spectrum in HG are fitted with gaussian distributions, and from the peak-to-peak distance a conversion factor from ADC to photo-electrons (p.e. in the following) was determined. A typical conversion factor was about 1 p.e./ADC count with uncertainties of the order of 0.1%.

- The pedestals of both the LG and HG are determined from a fit to the pedestal peak in evnts where the SiPM is not illuminated.

- The signal in the SiPM in a set of 40 GeV positron events was recorded for both teh LG and the HG. The LG signal was plotted against that of the HG, as shown in Figure 5. A linear fit (with the pedestals fixed to those extracted independently) determines a conversion factor from HG to LG[2].

The procedure was performed for all SiPMs and the parameters were extracted multiple times during the test beam, and the findings about stability of the SiPM calibrations of Ref. [17] were

[2]The fit to Figure 5 can also be done leaving the pedestals of LG floating to be determined by the fit. This was tried, and the results are consistent with those extracted independently.

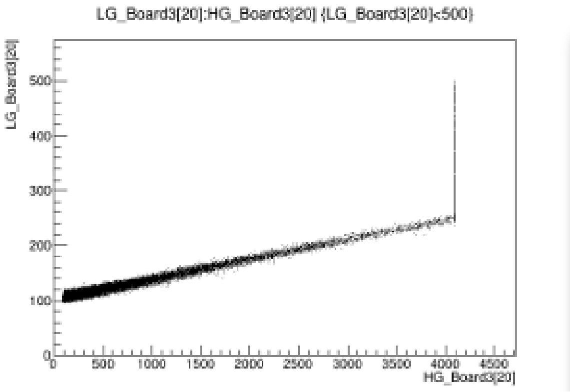

Figure 5. Scatter plot of HG (in p.e.) signal against the LG signal for the same SiPM.

confirmed. Given the stability of the calibration parameters over time, a single set of calibration constant for each SiPM was used for the whole data taking period. The signal used in the following for the data analysis is the SiPM signal in p.e. from the HG, unless the HG is found to be saturated, in which case the LG signal in p.e. is used.

It is well known [**?**] that SiPM yield a non-linear response to the incoming light when the number of photons in the pulse is a signficant fraction of the number of cells available for the SiPM. In this case, a standard procedure is to correct the SiPM response using the following formula:

$$N_{\text{fired}} = N_{\text{cells}} \times \left(1 - e^{-\frac{N_{\text{photons}} \times \text{PDE}}{N_{\text{cells}}}}\right)$$

Here N_{cells} is the number of cells available for the SiPM (7284 for the S14160-1315), N_{fired} is the recorder signal in p.e., N_{photons} is the number of photons that hit the cathode. By inverting this relation, the SiPM response can be corrected to account for non-linearities. This procedure was implemented to correct for the SiPM response. For example, this correction was at the level of 5% when a signal of 2 GeV was measured in a single scintillating fibre.

4.2 Calorimeter response equalisation

Next, the response of the $\text{M}_0 - \text{M}_8$ modules was equalised using a beam of positrons with a momentum of 20 GeV. The beam was centered in the geometrical centre of each module. A well-centered, high-purity positron beam can be obtained by applying the positron selection of Section 3. The equalisation procedure assumed an equal tower response to positrons, in runs where the beam is hitting the module centre. The equalisation was obtained by setting the response of all modules equal to that of M_0. In other words, if we define the response in p.e. of M_0 when hit in its centre by a beam of 20-GeV positrons as $P^{S,C}_{\text{M}_0}$ (20 GeV) (where the letter S or C represents scintillation or Cherenkov), then the response (in p.e.) of the i-th module M_i is obtained by shooting the beam at its own centre, measuring its response in ADC $A^{S,C}_{\text{M}_i}$, and computing a constant $a^{S,C}_i$ so that

$$P^{S,C}_{\text{M}_i}\ (20\ \text{GeV}) = a^{S,C}_i \times A^{S,C}_{\text{M}_i}\ (20\ \text{GeV}) = P^{S,C}_{\text{M}_0}\ (20\ \text{GeV})\,,$$

The containment of a single module to a 20-GeV positron beam is estimated to be $\epsilon_{\text{module}} = 72\%$ with the help of the Geant4 test beam simulation.

4.3 Calorimeter calibration

The overall calorimeter electromagnetic energy scale was set by rescaling the sum of the responses of the modules $M_0 - M_8$ by a single pair of common constants δ_S for the scintillation signal and δ_C for the Cherenkov signal, so that the total energy measured in the calorimeter corresponded to the beam energy separately for the scintillation and Cherenkov signal[3]. The constants δ_S and δ_C are determined as

$$\delta_{S,C} = \frac{20\ \text{GeV}}{\langle \sum_{i=0}^{8} P_{\text{M}_i}^{S,C} \rangle},$$

where the average is computed over all selected positrons from a 20-GeV run with the beam pointing to the geometric centre of M_0.

4.4 Refined offline analysis calibration

After the data taking was completed, it was noted that there was a small offset, at the level of about 5%, between the two readout responses (Cherenkov and scintillating). A possible explanation may stem from the fact that the shower containment of a single module as seen by the scintillating or Cherenkov readout is different (the shower is wider for the Cherenkov component, leading to a larger lateral leakage [17]).

A final calibration step was therefore performed during the analysis phase, independently for the Cherenkov and scintillating readouts. The total energy in a given event is defined as

$$E_{S,C} = \delta_{S,C} \sum_{0}^{8} \beta_i^{S,C} P_{\text{M}_i}^{S,C} + \beta_9 S_{\text{Ps}}$$

where S_{Ps} is the signal recorded for the pre-shower scintillator.

The coefficients $\beta_i^{S,C}$ are computed analytically by requiring that the distribution of $E_{S,C}$ has a mean value of 20 GeV when computed over a run where the beam was hitting the prototype at the nominal centre of $M_(0)$.

The distribution of the 18 $\beta_i^{S,C}$ values is within 15% of 1, with the exception of β_9, which serves a different purpose. The contribution of the energy loss in the preshower detector is estimated to be 80 MeV/MIP to be confirmed.

The energy distribution as measured by the calorimeter in response to a 20-GeV positron beam is shown in Figure 6

[3]The simulation predicts a shower containment of the full prototype of $\epsilon = 94\%$ at $E_{\text{beam}} = 20$ GeV. This number was found to be nearly independent with E_{beam}. This lateral leakage was therefore de-facto reabsorbed in the determination of $\delta_{S,C}$.

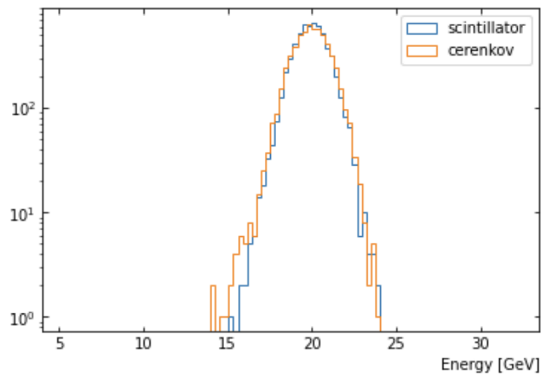

Figure 6. Energy measurement of the calorimeter after the full calibration procedure is applied. The results are shown separately for the Cherenkov (in yellow) and scintillation (in blue) channels.

4.5 Noise determination

The electronic noise contribution from the PMTs reading modules M_1-M_8 was estimated simply by making use of the pedestal triggers. The RMS of the pedestal combined energy distribution of the sum of the PMTs was estimated to be 120 MeV.

The estimate of the SiPMs contribution to the noise is trickier: because of the self-triggering system of the FERS, there is essentially no data from the FERS associated with pedestal triggers. Therefore, the multiphoton distribution in events with low energy deposit in the calorimeter were used instead. The noise was determined to be about 2 MeV for HG and 50 MeV for LG for the Cherenkov channels, and about 0.6 MeV for HG and 12 MeV for LG for the scintillation channels. The noise is found to be highly correlated between channels read out by the same FERS board, and loosely correlated for channels sitting odifferent FERS. The exact level of correlation depends on the FERS considered. Altogether, it was estimated that the total contribution to the noise of the cintillation (Cherenkov) SiPM to be of about 30 (90) MeV for the HG. The contribution from LG is more difficult to estimate, as typically there are only a handful of channels for which teh LG is used (and this number is of course energy dependent).

Taking everything into account, the total electronic noise contribution (from PMTs and SiPM) to the combined energy measurement is estimated to be about 150 MeV at 10 GeV and 250 GeV at 120 GeV.

5 Results

Following calibration, the data were analysed, and, similarly to Ref. [17], the performance of the prototype was characterised in terms of linearity and resolution of the energy response. For the latter in particular, the much improved positron beam purities at all energies, on top of a closer placement of the pre-shower detector to the calorimeter led to a complete assessment of the calorimeter resolution to positrons with beam energies from 10 to 120 GeV.

5.1 Positron energy measurement

As predicted in Ref. [17], the placement of the calorimeter with a tilt angle both in the $x - z$ and in the $y - z$ plane lead to a calorimeter response independent from the impact point of the particle on the calorimeter's front face do we have a plot that demonstrates this?. Following the calibration procedure described in Section 4, the combined dual-readout response of the calorimeter E was computed as the arithmetic average of the Cherenkov and scintillating channels, $E = (E_S + E_C)/2$.

As an example, the combined energy response to a positron beam of 20 and 80 GeV is shown in Figure 7.

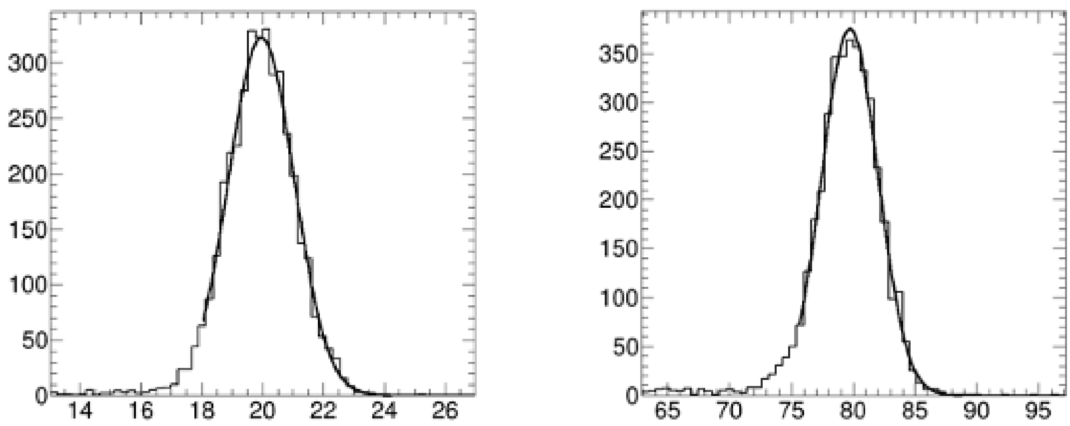

(a) (b)

Figure 7. Distribution of the combined energy response for positron beam energies of (a) 20 GeV and (b) 80 GeV.

The distributions are centred at the nominal beam energies as expected following the calibration procedure. The distributions are very close to gaussians in their core. Similar histograms were produced for all the available beam energies. In each case, the histograms were fit with a gaussian between $m - 1.8 \times r$ and $m + 4 \times r$, where m represents the mean value of the distribution and r its RMS. We name the mean of the resulting gaussian as E_{meas} and its sigma as σ.

A low energy tail (due to a non-complete rejection of particles other than positrons in the beam) can be observed. Its impact on the determination of the values of E_{meas} and σ was found to be negligible to be confirmed.

5.2 Linearity of the prototype response

Similar histograms were produced for all the available beam energies. The linearity of the prototype response is defined as the fractional difference between the measured and the beam energy, with respect to the beam energy, that is $(E_{\mathrm{meas}} - E_{\mathrm{beam}})/E_{\mathrm{beam}}$. It is shown as a function of E_{beam} in Figure 8 (a). The linearity of the response was better than 1% over the full explored range, with the exception of the point at E_{beam} = 10 GeV, where, however, the beam momentum and composition were less clear è vera questa cosa?.

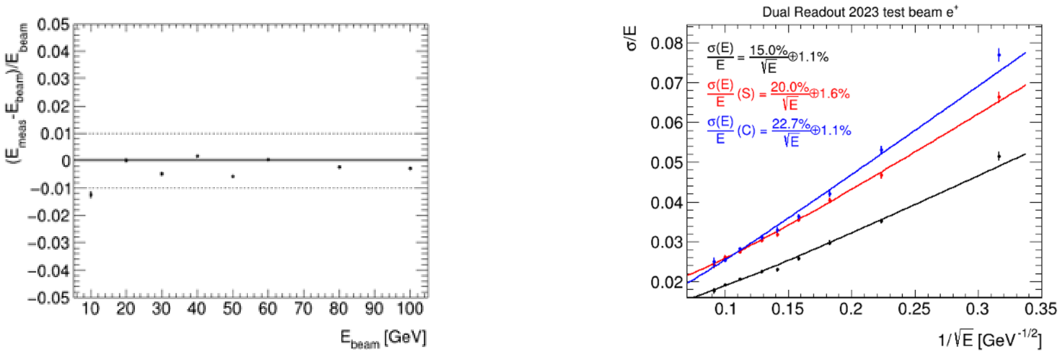

(a) (b)

Figure 8. (a) Linearity and (b) resolution of the calorimeter response on the beam energy. For (b), the independent resolutions of the Cherenkov (in blue) and scintillation (in red) channels are shown, together with the one on the combined response (in black).

5.3 Energy measurement resolution

Here we need to decide how to add the discussion about the noise. It is missing completely at the moment.

One of the key improvements of this paper with respect to Ref. [17] is the assessment of the calorimeter resolution with real data. In Ref. [17], a poor positron purity of the beam, together with a non-ideal placement of the pre-shower scintillator with respect to the calorimeter forced us to assess the calorimeter energy resolution to positrons at energies above 30 GeV checK by making use of the test beam software simulation, after making sure that the results were compatible with real data at low energies.

We define the resolution of the energy measurement as the ratio of σ to E_{meas}. It is shown in Figure 8 (b). The Cherenkov, scintillation, and combined resolutions as a function of the beam energy are fit with a function of the type

$$\frac{\sigma}{E_{\text{meas}}} = \frac{a}{\sqrt{E_{\text{meas}}}} \oplus b$$

where E_{meas} is expressed in GeV. The fit to the combined response curve yielded a value of the stochastic term $a = 15.0\%$ and of the constant term $b = 1.1\%$.

A direct comparison with the curve obtained with the test beam software simulation assuming ideal test beam conditions obtained in Ref. [17] is shown in Figure 9. The result indicates a slightly worse resolution overall. However, this seems to be due to an overall worse constant term b, rather than a difference in the stochastic term. Indeed, further investigations brought us to attribute this difference in constant term mainly to the spread in beam momentum, which is estimated to be of the order of 1.5% to be ckecked.

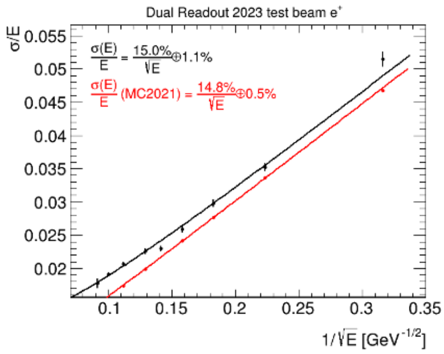

Figure 9. Distribution of the energy measured after all corrections for a 20-GeV positron beam for (a) data and (b) the simulation.

In conclusion, the investigation of the energy resolution with positrons confirms the assessment done with help of the software simulation of the test beam in Ref. [17].

6 Conclusions

A dual-readout sampling calorimeter prototype using brass capillary tubes as absorber and optical fibres as active medium was tested using beams of particles at the H8 beam line at CERN. The dual readout was realised by making use of two different types of fibres: doped scintillating Saint-Gobain BCF-10 fibres, and clear "Cherenkov" Mitsubishi SK40 fibres. The prototype (with a total size of about $10 \times 10 \times 100$ cm^3) was composed by nine modules. For the central module, the individual fibres were read out by means of Hamamatsu S14160-1315 PS SiPMs, while for the surrounding eight modules the two sets of fibres were bundled together and read out by Hamamatsu R8900 PMTs.

The detector was calibrated by making use of the SiPM multiphoton spectrum and of beams of positrons. Then, the detector response was studied using beams of positrons with energies between 10 and 120 GeV. Thanks to the excellent beam purity, at all beam energies, it was possible to assess the detector response in terms of linearity and resolution of the energy measurement. The linearity was found to be within 1%. The energy resolution was found to be

$$\frac{\sigma}{E} = \frac{15.0\%}{\sqrt{E}} \oplus 1.1\%,$$

in agreement with what was estimated with a geant4 simulation of the detector validated at previous test-beams for ideal test-beam conditions, after taking into account the beam momentum spread.

The results on the electromagnetic performance of the dual-readout sampling calorimeter described in this paper confirm that the capillary tube mechanical solution in conjunction with a SiPM based readout is a viable solution for future developments, and pave the way to the use of this technology for use in a prototype with a size able to contain the hadronic shower. The work is ongoing under the HiDRa project [**?**] find a suitable citation for hidra.

References

[1] S. Lee, M. Livan and R. Wigmans, *Dual-Readout Calorimetry*, *Rev. Mod. Phys.* **90** (2018) 025002 [1712.05494].

[2] FCC collaboration, *FCC-ee: The Lepton Collider: Future Circular Collider Conceptual Design Report Volume 2*, *Eur. Phys. J. ST* **228** (2019) 261.

[3] CEPC Study Group collaboration, *CEPC Conceptual Design Report: Volume 2 - Physics & Detector*, 1811.10545.

[4] N. Akchurin, K. Carrell, H. Kim, R. Thomas, R. Wigmans, J. Hauptman et al., *Electron detection with a dual-readout calorimeter*, *Nucl. Instrum. Meth. A* **536** (2005) 29.

[5] N. Akchurin, K. Carrell, J. Hauptman, H. Kim, H.P. Paar, A. Penzo et al., *Hadron and jet detection with a dual-readout calorimeter*, *Nucl. Instrum. Meth. A* **537** (2005) 537.

[6] N. Akchurin, K. Carrell, H. Kim, R. Thomas, R. Wigmans, J. Hauptman et al., *Comparison of high-energy electromagnetic shower profiles measured with scintillation and Cherenkov light*, *Nucl. Instrum. Meth. A* **548** (2005) 336.

[7] N. Akchurin et al., *Dual-readout Calorimetry*, 1307.5538.

[8] S. Lee et al., *Hadron detection with a dual-readout fiber calorimeter*, *Nucl. Instrum. Meth. A* **866** (2017) 76 [1703.09120].

[9] N. Akchurin et al., *The electromagnetic performance of the RD52 fiber calorimeter*, *Nucl. Instrum. Meth. A* **735** (2014) 130.

[10] M. Antonello et al., *Tests of a dual-readout fiber calorimeter with SiPM light sensors*, *Nucl. Instrum. Meth. A* **899** (2018) 52 [1805.03251].

[11] L.Pezzotti, *Particle Detectors R&D: Dual-Readout Calorimetry for Future Colliders and MicroMegas Chambers for the ATLAS New Small Wheel Upgrade*, Ph.D. thesis, Universitá degli Studi di Pavia, 2021.

[12] I. Pezzotti et al., *Dual-Readout Calorimetry for Future Experiments Probing Fundamental Physics*, 2203.04312.

[13] M.T. Lucchini, W. Chung, S.C. Eno, Y. Lai, L. Lucchini, M.-T. Nguyen et al., *New perspectives on segmented crystal calorimeters for future colliders*, *JINST* **15** (2020) P11005 [2008.00338].

[14] M.T. Lucchini, L. Pezzotti, G. Polesello and C.G. Tully, *Particle flow with a hybrid segmented crystal and fiber dual-readout calorimeter*, *JINST* **17** (2022) P06008 [2202.01474].

[15] G. Gaudio, *The IDEA detector concept for FCCee*, *PoS* **ICHEP2022** (2022) 337.

[16] A. Karadzhinova-Ferrer et al., *Novel prototype tower structure for the dual-readout fiber calorimeter*, *JINST* **17** (2022) T09007.

[17] N. Ampilogov et al., *Exposing a fibre-based dual-readout calorimeter to a positron beam*, *JINST* **18** (2023) P09021 [2305.09649].

[18] D.L. Chichester, S.M. Watson and J.T. Johnson, *Comparison of bcf-10, bcf-12, and bcf-20 scintillating fibers for use in a 1-dimensional linear sensor*, in *2012 IEEE Nuclear Science Symposium and Medical Imaging Conference Record (NSS/MIC)*, pp. 365–370, 2012, DOI.

[19] Mitsubishi ESKA SK40. https://www.pofeska.com/pofeskae/download/pdf/f/SK40.pdf, accessed on 14 March 2023.

[20] HAMAMATSU R8900. https://www.hamamatsu.com/content/dam/hamamatsu-photonics/sites/documents/99_SALES_LIBRARY/etd/R8900(U)-00-C12_TPMH1299E.pdf, accessed on 14 March 2023.

[21] HAMAMATSU S14160-1315PS. https://www.hamamatsu.com/jp/en/product/optical-sensors/mppc/mppc_mppc-array/S14160-1315PS.html, accessed on 16 March 2023.

[22] FERS A5202, CAEN S.p.A., FERS A5202. https://www.caen.it/products/a5202/, accessed on 18 January 2023.

[23] Citiroc-1A. https://www.weeroc.com/products/sipm-read-out/citiroc-1a, accessed on 18 January 2023.

[24] Linear Collider CERN Detector collaboration, *Particle Identification with Cherenkov detectors in the 2011 CALICE Tungsten Analog Hadronic Calorimeter Test Beam at the CERN SPS*, *LCD-Note-2013-006, AIDA-NOTE-2015-012* (2013) .